

Supporting Information for

Extremely Elevated Room-Temperature

Kinetic Isotope Effects Quantify the Critical

Role of Barrier Width in Enzymatic C-H

Activation

Shenshen Hu,^{†,§,‡} Sudhir C. Sharma,^{†,§,‡} Alexander D. Scouras,^{§,&} Alexander V. Soudackov[#], Cody A. Marcus Carr,^{†,§,-} Sharon Hammes-Schiffer,[#] Tom Alber,^{§,&} Judith P. Klinman^{*,†,§,&}

[†]Department of Chemistry, University of California, Berkeley, California 94720, U.S.A.

[&]Department of Molecular and Cell Biology, University of California, Berkeley, California, 94720, U.S.A.

[§]California Institute for Quantitative Biosciences, University of California, Berkeley, CA 94720, U.S.A.

[#]Department of Chemistry, University of Illinois at Urbana-Champaign, 600 South Mathews Avenue, Urbana, IL 61801, U.S.A.

Contents

I. Materials and Methods

- 1.1 Mutagenesis, Expression and Purification of DM SLO
- 1.2 Steady-State Kinetics Assays of the DM SLO.
- 1.3 Pre-Steady-State Kinetics Assays of the DM SLO.
- 1.4 Enzyme Stability for Steady-State Kinetics.
- 1.5 Enzyme Stability for Pre-Steady-State Kinetics.
- 1.6 Crystallization, Data Collection and Crystallographic Refinement.
- 1.7 Non-adiabatic Fitting for WT, I553 series mutant and DM SLO

II. Figures S1–S10

III. Table S1–S4

IV. References (1–22)

I. Materials and Methods

1.1 Mutagenesis, Expression and Purification of DM SLO

The DM SLO plasmid was prepared following the Stratagene QuikChange II protocol starting from the L546A SLO plasmid with mutation at position A754 using the forward: 5'-CTT TCA GTG ATA GAG ATC GCA TCG ACA CAT GCT TCT-3' and reverse: 5'-AGA AGC ATG TGT CGA TGC GAT CTC TAT CAC TGA AAG-3' primers. The mutant plasmids were isolated and the double mutation confirmed by sequencing with three different primers that targeted different regions of the gene: the beginning of the gene, a 500-bp region of the gene containing the mutation site(s) and a region that covers 500-bp up to the end of the gene.

These double mutants were expressed using the pT7-7 plasmid in *E. coli* and purified as described before with some minor modifications¹⁻³. The starting culture was diluted 300-fold and incubated at 37°C with shaking until OD600 reached ~0.7. The temperature was then rapidly lowered to 15°C and incubated with shaking for an additional 96 h. The cells were harvested and stored at -80°C until purification.

Cell paste from 3 L (~18 g) was resuspended in *ca.* 72 mL lysis buffer [25 mM Tris-base (pH 7.5), 0.1 mM EDTA, 1× BugBuster (Novagen), 1250 units of benzonase (Novagen), ~0.5 mM aminoethylbenzenesulfonyl fluoride (Sigma) and ~0.2 mg/mL of lysozyme (Sigma)]. The lysis reaction was allowed to proceed for 40 min at RT followed by cooling to 4°C for 20 min. The lysis mixture was centrifuged at 20,000 rpm for 20 min to pellet the insoluble cellular debris. The soluble supernatant was dialyzed in 20 mM Bis-Tris (pH 6) for 3 to 4 h, centrifuged and then loaded to a column packed with 70 mL SP Sepharose fast flow (Sigma). The column was then washed with 100 mL of 20 mM BIS-TRIS (pH 6) buffer until the absorbance at 280 nm reached zero. The bound proteins were eluted with a 600 mL linear gradient from 0 to 500 mM NaCl (Solution A: 20 mM BIS-TRIS (pH 6); Solution B: 20 mM BIS-TRIS (pH 6), 500 mM NaCl). The fractions containing SLO (identified via SDS-PAGE and monitoring of enzyme activity) were pooled and further dialyzed in 20 mM BIS-TRIS (pH 6), to remove salt. Protein was then concentrated and further purified using an UNO S6 column (Biorad) with a 210 mL step-wise gradient from 0 to 500 mM NaCl in 20 mM BIS-TRIS (pH 6). The enzyme-containing fractions were pooled, buffer exchanged in 100 mM borate (pH 9.0) and concentrated to minimal volume. SLO double mutants were routinely obtained with a final yield of *ca.* 6 mg/L of cells. The purity of the enzymes was greater than 90% as seen by SDS-PAGE.

1.2 Steady-State Kinetics Assays of the DM SLO.

Steady-state kinetics with protio-LA were performed on a Cary50 spectrophotometer in the single wavelength mode. The reaction progress was monitored by following the generation of the product, 13-(S)-HPOD ($\epsilon_{234} = 23,600 \text{ M}^{-1} \text{ cm}^{-1}$). The assays were performed in 100 mM borate (pH 9.0) under ambient atmosphere in a constant

temperature regulated by a water-jacketed cuvette holder as described previously with some minor adjustments⁴. The substrate concentration ranged from 0.70 to 35 μM . Kinetic reactions were initiated by the addition of small aliquots of enzyme, with final concentrations of 0.6–1 μM for DM SLO. The UV kinetic profile shows a lag phase, which gradually decreases on either increasing the substrate concentration or increasing the assay temperature and becomes much smaller for reactions performed at higher temperatures ($T \geq 45^\circ\text{C}$) with higher concentrations (above 20 μM) LA. The lag phase is followed by a linear rate, which in turn is followed by a steady decrease in the reaction rate as the substrate concentration is depleted. The initial rates were fitted to the Michaelis-Menten equation to obtain the unimolecular kinetic parameter k_{cat} (Table S1). The errors associated with each k_{cat} measurements were used to weigh the exponential Arrhenius fit. A second, discontinuous method involved reaction of protio- or d_2 -LA with DM SLO in 0.1 M borate, pH 9.0, at 30°C . At different time points, aliquots were acid quenched (final acetic acid concentration in the mixture $\sim 5\%$) and extracted with methylene chloride (3 extractions, 3 mL each). The methylene chloride layer was evaporated, the residue redissolved in methanol and RP-HPLC used for separation of the product hydroperoxides. The reactions were performed with 0.6–1 μM enzyme at a substrate concentration of 33 μM . The protio-LA showed maximal rate in the spectrophotometric assay at that concentration. This was also saturating for deuterated substrate which always shows a reduced K_m relative to the unlabelled LA. The integrated peak area representing each product hydroperoxide equates to the amount of the product generated at the specific time points of an aliquot. A time course of the product formation is obtained and a slope is calculated from the change in peak area at 234 nm. The KIE is then calculated from the ratio of slopes for product formation (protio-LA: d_2 -LA), corrected for the different concentrations of enzyme used in the separate assays.

1.3 Pre-Steady-State Kinetics Assays of the DM SLO

The pre-steady state kinetics for protio-LA were performed on a Cary-50 spectrophotometer under a single wavelength mode (330 nm) at a constant temperature (30°C) regulated by a water-jacketed cuvette holder. Ferric SLO, the active protein, was prepared *in situ* in the cuvette before each measurement by the addition of 2 equiv. of 13-(*S*)-HPOD in the presence of air. The cuvette was then placed into the glove box. Glucose oxidase, catalase and glucose stock (N_2 -saturated) were added subsequently. The cuvette containing 60 μM DM SLO was capped by a rubber stopper before removal from the glove box. After 10 min, reaction was initiated by the rapid addition of an equal volume of protio-LA stock solution (480 μM) with gastight syringe, to give a final concentration of 30 μM DM SLO, 240 μM substrate, 50 units/mL glucose oxidase, 250 units/mL catalase and 50 mM glucose. The disappearance of absorbance vs. time for protio-LA could be directly fit to single exponential decay process (Figure S7).

The comparative pre-steady-state kinetics for protio-LA and d_2 -LA were performed on a Hewlett-Packard 8453 UV spectrophotometer in the glove box under a single

wavelength mode (330 nm) with a constant temperature of 35°C. Ferric SLO was first prepared *in situ* in the cuvette before each measurement by the addition of 2 equiv. of 13-(*S*)-HPOD to the SLO solution in the presence of air, during which the increase in absorbance could be directly observed on a Cary50 spectrophotometer. The cuvette was then placed into the glove box. Glucose oxidase, catalase and glucose stock (N₂-saturated) were added subsequently. The cuvette, containing 60 μM DM SLO, was capped with a glass stopper. After a 10 min incubation, reaction was started by the rapid addition of an equal volume of either H-LA or *d*₂-LA stock solution (480 μM) with a syringe, to give a final concentration of 30 μM DM SLO, 240 μM substrate, 50 units/mL glucose oxidase, 250 units/mL catalase and 50 mM glucose. The cuvette was further sealed with a glass stopper and high-vacuum grease. For these pre-steady kinetic traces in the glove box, the UV-vis spectrophotometer was reset to zero before adding the substrates, which led to negative absorbance changes for protio-LA and *d*₂-LA (Figure 2C and 2D). We note that the overall decrease in the absorbance for the substrate-based decay was variable and generally less than the maximum value expected from the increase in absorbance during the pre-activation process (*ca.* ~0.05 Abs). This is attributed to differences in UV-vis instrumentation, sample handling, time between oxidation and degassing and the addition of substrate, *etc.* Importantly, when H and D substrates were analyzed side by side, the same degree of decrease in absorbance was observed.

1.4 Enzyme Stability for Steady-State Kinetics

A number of controls were conducted to ascertain whether DM SLO was prone to inactivation during the long lag phase. These involved extended incubations of DM SLO either in the presence of a concentration of enzyme or substrate equal to that used in the kinetic assays, *ca.* 1 μM enzyme (with 1 μM *d*₂-LA) or *ca.* 30 μM substrate (with 30 μM enzyme). These conditions allowed the dilution of pre-incubated enzyme into assays that contained a final concentration of *d*₂-LA that was only *ca.* 3% of the protio-substrate, circumventing enzyme inhibition in assays of protio-LA turnover. As shown in Extended Data Fig. 6A and S6B, there is no evidence for a significant loss of enzyme activity after very long periods of time. Although the enzyme is subject to inactivation by prolonged incubation with high levels of the product, protio-HPOD, hydroperoxide was neither detected nor expected during the extensive lag period, Figure S6C.

1.5 Enzyme Stability for Pre-Steady-State Kinetics.

Ferric SLO, the active protein, was prepared *in situ* in the vial by the addition of 2 equiv. of 13-(*S*)-HPOD to the SLO solution in the presence of air. The active enzyme was then incubated under strict anaerobic conditions in the glove box at a concentration of *ca.* 30 μM at 30°C. At the indicated time points, enzyme was taken out of the glove box, diluted and assayed for activity with the protio-LA substrate. As shown in Extended Data Fig. 8, there is no evidence for a significant loss of enzyme activity after very long periods of time.

1.6 Crystallization, Data Collection and Crystallographic Refinement.

Samples of SLO for crystallization were further purified by size-exclusion chromatography. Protein prepared as described above was dialyzed against three changes of 50 mM sodium acetate, pH 5.0, for 1 h each, which resulted in the formation of a moderate amount of precipitate which was removed by centrifugation. The supernatant was then loaded on a GE Superdex 200 10/300 GL column (held at room temperature) and eluted with 50 mM HEPES and 150 mM sodium chloride, pH 7.4, at a flow rate of 0.5 mL/min. Fractions containing SLO were pooled, concentrated to 4.5–5.0 mg/mL, dialyzed against three changes of 50 mM sodium acetate, pH 5.0, as above and used immediately for crystallization.

Crystals of SLO were grown as previously described⁵, with minor modifications. Sitting drops (5 μ L of 4 mg/mL enzyme in 50 mM sodium acetate, pH 5.0, and 5 μ L well solution) were equilibrated against 500 μ L of well solution (9% PEG3350, 200 mM sodium acetate, pH 5.5). Drops were microseeded after 1 hour; *de novo* crystals could be generated in similar conditions, optionally increasing PEG or protein concentrations. Crystal quality was improved over three generations of seeding. The best crystals reached 300 \times 300 \times 500 μ m after a few days. For cryoprotection, crystals were transferred in five steps to a solution of 20% PEG3350, 200 mM NaOAc, pH 5.5, and 20% ethylene glycol and then flash frozen in liquid nitrogen.

Diffraction data were collected at 100 K at Beamline 8.3.1 of the Advanced Light Source at Lawrence Berkeley National Laboratory. All data were processed by the Elves program⁶, with integration performed in MOSFLM⁷ and scaling and merging in SCALA, POINTLESS and TRUNCATE^{8, 9}. An initial solution was found by molecular replacement using Phaser¹⁰ with PDB 3PZW as the search model. Manual refinement was performed in *Coot*¹¹ and automated refinement using the *PHENIX* suite¹². 3PZW was rerefined under identical parameters as the WT control structure. Complete refinement statistics for DM SLO can be found in Table S4.

1.7 Non-adiabatic Fitting for WT, I553 series mutant and DM SLO

The rate constants and kinetic isotope effects (KIEs) were calculated using the nonadiabatic proton-coupled electron transfer (PCET) rate constant expression. On the basis of a thermodynamic analysis¹³ and density functional theory calculations,¹⁴ the SLO reaction is thought to occur through a concerted PCET mechanism involving the transfer of an electron from the π -system of the substrate to the iron of the cofactor and a proton from the C11 carbon of the substrate to the hydroxyl ligand of the cofactor. The electron donor and acceptor are spatially separated from the proton donor and acceptor, with a significant electron donor-acceptor distance. Moreover, an orbital and spin density analysis indicates that the electron transfers directly from an orbital localized on the substrate to an orbital localized on the iron without ever becoming localized on the proton.¹⁴ According to this analysis, the SLO reaction is qualitatively similar to other

reactions that have been shown rigorously to exhibit significant electron-proton nonadiabaticity.¹⁵⁻¹⁷ Thus, this reaction is likely to be nonadiabatic according to the definitions and diagnostics discussed elsewhere¹⁵⁻¹⁷ and can be modeled with the rate constant expression given in Eq. (S1) below.

The nonadiabatic PCET rate constant expression in the high-temperature (low-frequency) limit for the proton donor–acceptor vibrational mode is:¹⁶

$$k^{\text{PCET}} = \sum_{\mu} P_{\mu} \sum_{\nu} \frac{|V^{\text{el}}|^2 S_{\mu\nu}^2}{\hbar^2} \exp\left[\frac{2k_{\text{B}}T\lambda_{\mu\nu}^{(\alpha)}}{\hbar^2\Omega^2}\right] \sqrt{\frac{\pi}{k_{\text{B}}T(\lambda + \lambda_{\mu\nu}^{(\alpha)})}} \times \exp\left[-\frac{(\Delta G^{\circ} + \lambda + \lambda_{\mu\nu}^{(\alpha)} + \varepsilon_{\nu} - \varepsilon_{\mu})^2}{4(\lambda + \lambda_{\mu\nu}^{(\alpha)})k_{\text{B}}T}\right] \quad (\text{S1})$$

where the summations run over the reactant (μ) and product (ν) proton vibrational states with energies ε_{μ} and ε_{ν} , respectively, in the reactant and product proton diabatic potentials modeled by Morse functions; P_{μ} are the Boltzmann populations of the reactant proton vibrational states; V^{el} is the electronic coupling; $S_{\mu\nu}$ are the overlap integrals between the reactant and product proton vibrational wavefunctions; Ω is the effective frequency of the proton donor-acceptor vibrational mode; $\lambda_{\mu\nu}^{(\alpha)} = \hbar^2\alpha_{\mu\nu}^2/2M$ is the coupling reorganization energy, which depends on the coupling attenuation parameter $\alpha_{\mu\nu}$ and the effective mass M of the proton donor-acceptor vibrational mode; λ is the total reorganization energy; and ΔG° is the reaction free energy. In this paper, the electronic coupling is assumed to be the same for hydrogen and deuterium and therefore is not relevant to the calculation of the KIE. The effective mass M is assumed to be 100 amu, as in previous studies of SLO,^{19, 20} but the KIE has been shown to be insensitive to this parameter in this regime for the same force constant $M\Omega^2$.¹⁸ Comparison of the KIEs obtained with this expression to those obtained with a rate constant expression that is valid for all proton donor-acceptor frequencies (i.e., the proton donor-acceptor mode time correlation function is represented by that of a quantum mechanical harmonic oscillator) indicates that Eq. (S1) is valid for proton donor-acceptor frequencies up to $\sim 300 \text{ cm}^{-1}$ in the regime of physically reasonable parameters¹⁸.

The reactant and product diabatic potentials along the proton coordinate were modeled by standard Morse potentials given by

$$U_{XY}^{(\text{Morse})}(R_{XY}) = D_{XY} \left[e^{-2\beta_{XY}(R_{XY}-R_{XY}^0)} - 2e^{-\beta_{XY}(R_{XY}-R_{XY}^0)} \right] \quad (\text{S2})$$

where XY corresponds to the C–H and O–H bonds for the reactant and product diabatic potentials, respectively. The minima of the two Morse potentials associated with the reactant and product are separated by R_{eq} , the equilibrium proton donor–acceptor distance. The values for the Morse parameters for the C–H and O–H bonds in SLO were obtained

from our previous study¹⁸. The hydrogen and deuterium vibrational wavefunctions for the Morse potentials, as well as the overlap integrals between the reactant and product vibrational wavefunctions, were calculated analytically. The attenuation parameters $\alpha_{\mu\nu}$ were calculated with the finite difference method using the relation $\alpha_{\mu\nu} = -d \ln S_{\mu\nu} / dR$ evaluated at R_{eq} , the equilibrium value of R .

The reorganization energy, λ , has been chosen to reproduce the temperature dependence of the absolute rate constant for the wild type SLO (Figure S9A). Since the λ value is significantly smaller than the value used in earlier calculations, the proton donor–acceptor mode equilibrium distances and frequencies were recalculated using the experimentally determined temperature dependence of the KIE for WT⁴ and the single mutant series I553X (Table S2).⁵ We note that the obtained proton donor–acceptor equilibrium distances and frequencies (Table S2) are identical to the values calculated previously²⁰. Thus, the parameters that define the distance and sampling mode are independent of the reorganization energy (within the physically reasonable regime).

Two methods were employed to fit the temperature dependence of the absolute rate constant, $k_{\text{cat}}(\text{H})$, for the double mutant: (1) Adjustment of the reorganization energy (Figure S9B) and (2) introduction of a work term (W)^{21, 22} into the rate constant expression while keeping the reorganization energy the same as for the wild type SLO (Figure S9C). The work term is an additional temperature-dependent prefactor in the rate constant expression [$\exp(-W/k_{\text{B}}T)$] and does not depend on the isotope. Thus it affects the magnitude and temperature dependence of the rate constants for hydrogen and deuterium in the same manner and therefore cancels when the KIE is evaluated.

During this fitting of the absolute rate constant, the proton donor–acceptor mode equilibrium distances and frequencies remained fixed to the values calculated for WT (Table S3). Subsequently, R_{eq} and Ω were adjusted to reproduce the double mutant KIE (Figure 3 and Figure S10). As for WT and I553X (see above), the value assigned to λ does not affect the final values for R_{eq} and Ω . While $k_{\text{cat}}(\text{H})$ for the double mutant could be measured between 5 and 50°C, the extremely slow rate for DM SLO limited the present measurement of the KIE to 30°C (steady-state kinetics) and 35°C (pre-steady-state kinetics). Thus, the fitted proton donor–acceptor equilibrium distance and frequency can be assigned a range of values (Figure 3 and Figure S10) but not a single value.

II. Figures S1-S10

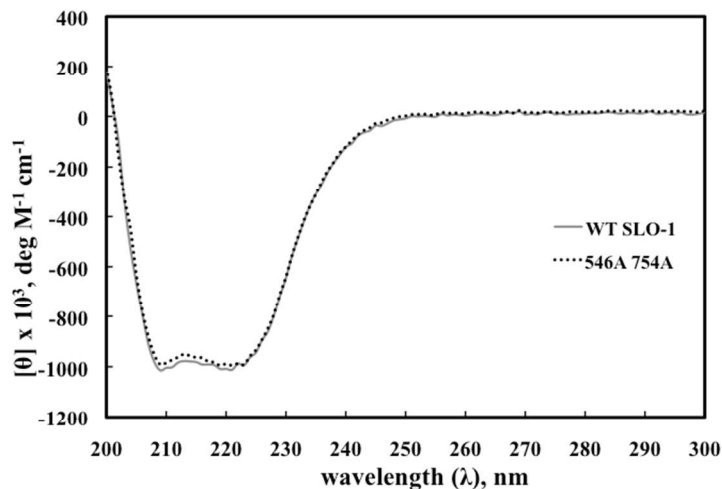


Figure S1. Circular dichroism (CD) analysis of WT and DM SLO. These measurements were carried out on an Aviv 410 spectro-polarimeter with a Peltier temperature-controlled cell holder using 1 cm pathlength cuvette. A 50 $\mu\text{g/mL}$ sample of either WT SLO or DM SLO in 0.1 M borate, pH 9.0, was equilibrated at 25°C for 5 min before recording the CD signals from 200 nm to 300 nm.

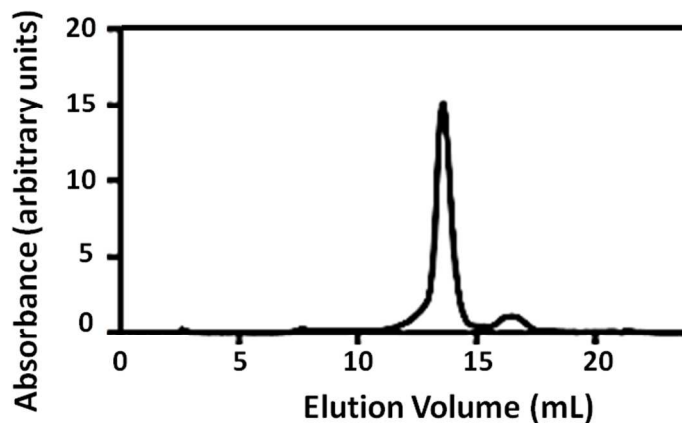


Figure S2. Size exclusion chromatography of DM SLO. The protein elutes as a monomer, corresponding to a spherical protein MW of 125 kDa. (The slightly larger mass is unsurprising given the ellipsoid shape of SLO.) No significant aggregation is observed. The small peak at 16.5 mL elution volume is a minor impurity that is observed in all preparations of SLO. Column conditions: GE Life Sciences Superdex 200 10/300 GL, 50 mM sodium borate, 150 mM sodium chloride, pH 9.0, at 0.5 mL/min. Injected 100 μL of 4 μM SLO.

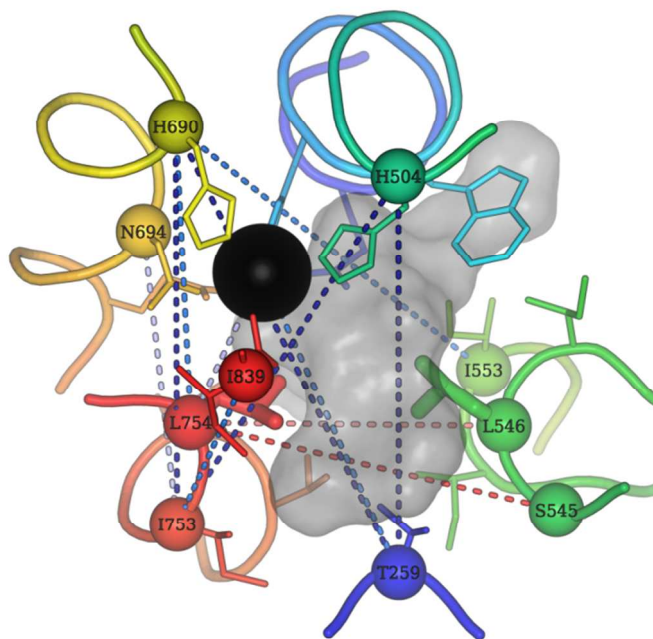
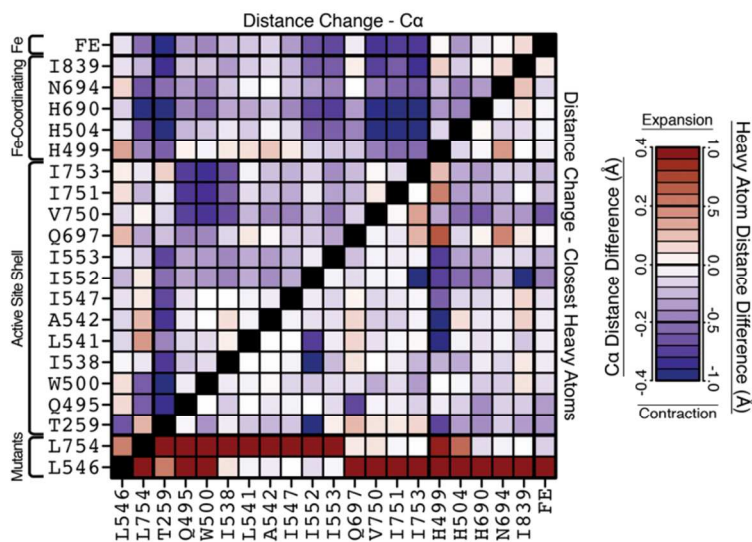


Figure S3. Changes in active site dimension of DM SLO. **(A)** Distance difference matrix for Ca atoms (top half) and closest heavy atom pair (bottom half) between each residue for selected residues and the Fe in the substrate binding site. The extensive blue color indicates small shifts of residues towards each other. In contrast, the substituted residues slightly move apart. Red rows for the mutant residues in the lower half reflect the expanded cavity due to a change to the respective Ala $\text{C}\beta$ as the closest atom. **(B)** The backbone at positions 754 and 546 of the double mutant expands *ca.* 0.26 \AA away (red horizontal lines). Meanwhile the backbones of the rest of active site move about 0.46 \AA (blue lines).

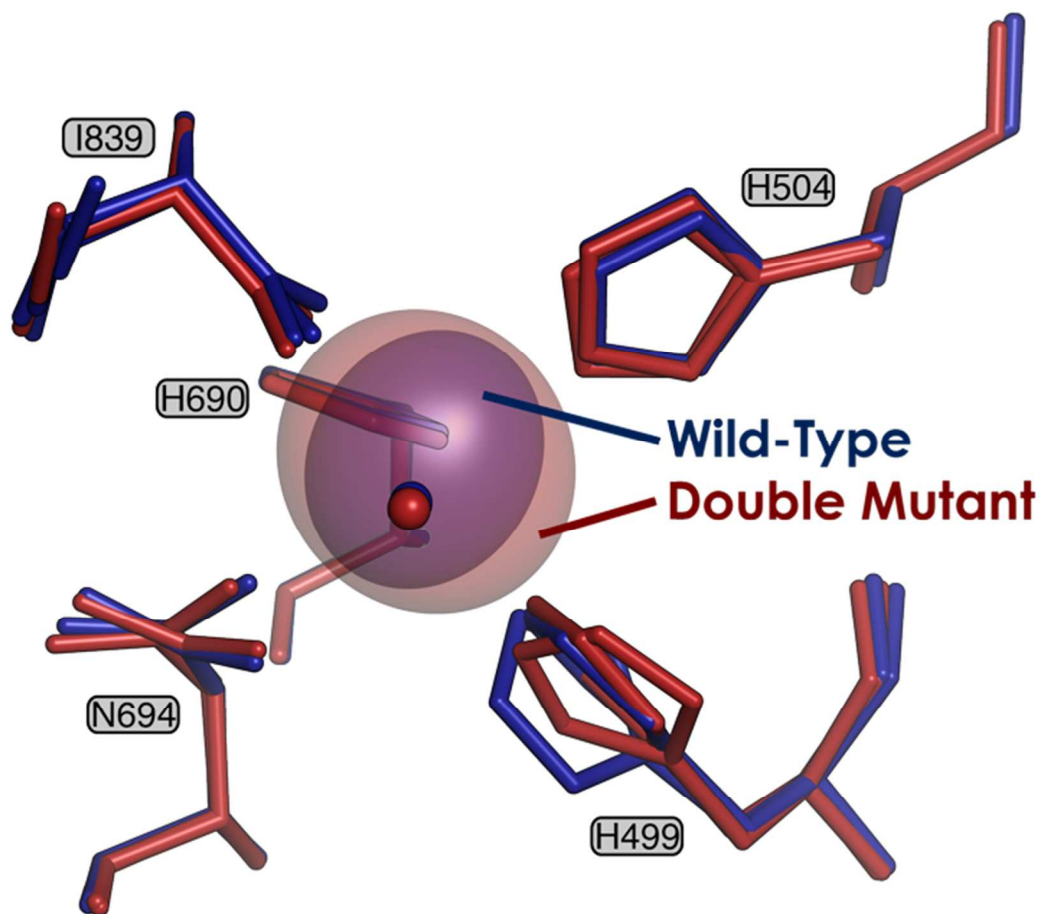


Figure S4. Superposition of the Fe-coordination residues in WT (blue) and DM (red) SLO. Fe atoms are represented by thermal ellipsoids. DM SLO Fe shows lower anisotropy, but the principal axis of vibration is rotated relative to that of WT SLO. The principal axes of both Fe atoms are orthogonal to the activated water (red sphere).

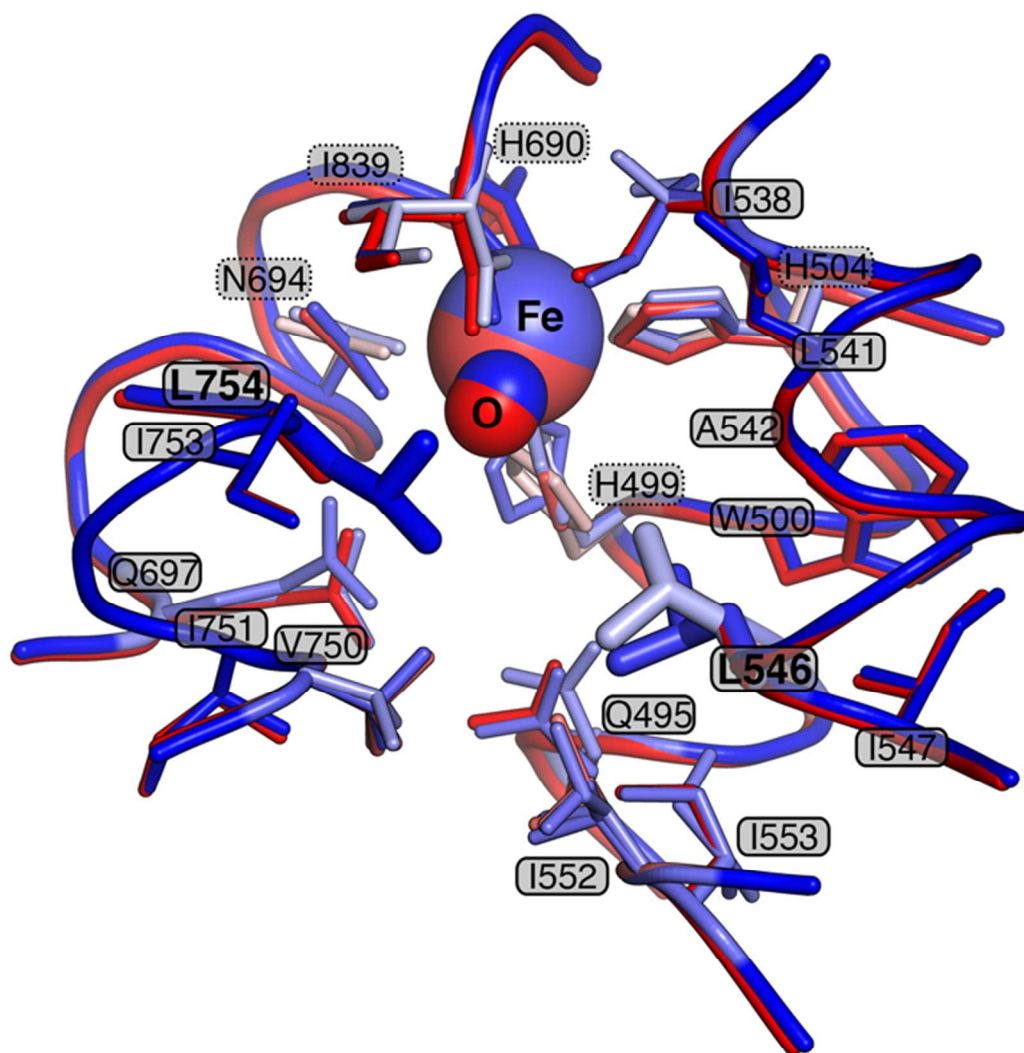


Figure S5. Superposition of the residues that form the cavity in WT (blue) and DM (red) SLO. Except for the expanded cavity, the DM preserves the topography of the active site. Alternate side-chain conformations are color saturated in proportion to their occupancy. The DM generally preserves the backbone position and side-chain conformational distribution. H499, I553, Q697, Q495, T259 (not shown) undergo changes in populations.

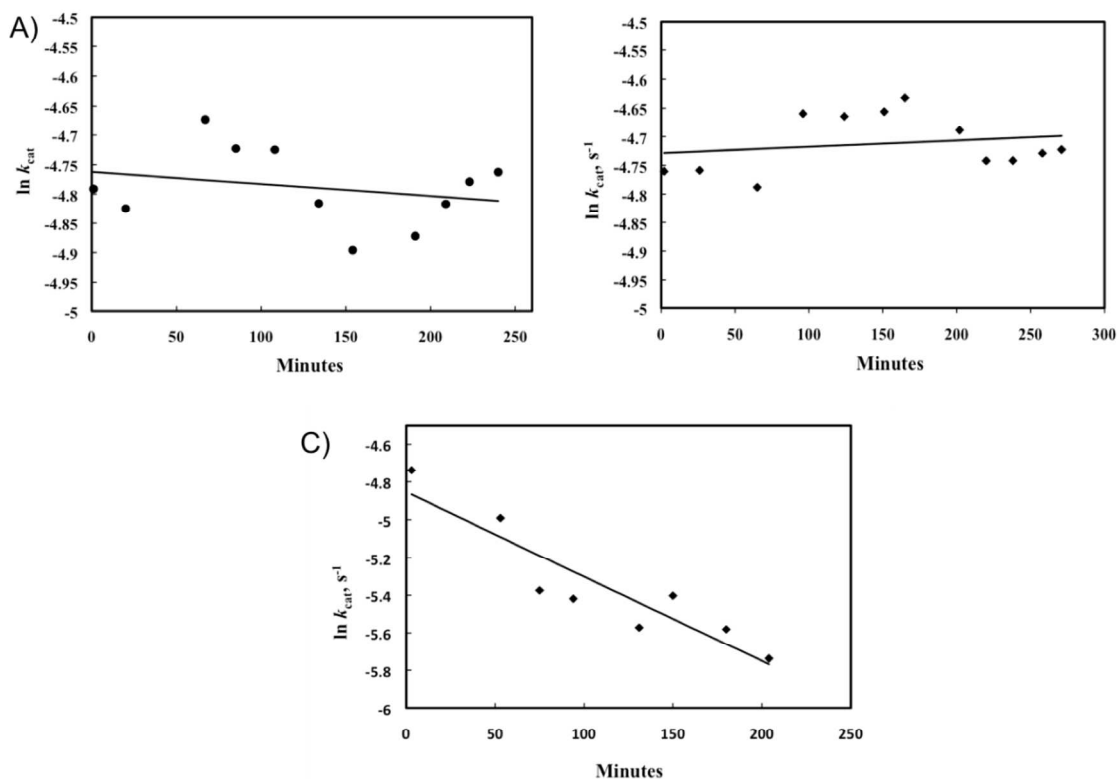


Figure S6. Stability of the DM SLO under conditions of the steady state assays. **(A)**. Assay in the presence of an equimolar amount of d_2 -LA and enzyme ($1.15 \mu\text{M}$ each) at 30°C , pH 9.0, 0.1 M borate. At the indicated time points, enzyme was diluted and assayed for activity with the protio-LA substrate. **(B)**. Incubation and assay of equimolar DM SLO and d_2 -LA ($26 \mu\text{M}$), as described in B above. **(C)**. A control reaction depicting the time-dependent loss of activity of DM SLO when incubated with product hydroperoxide (from protio-LA) in a 1:1 ratio (each at $26 \mu\text{M}$).

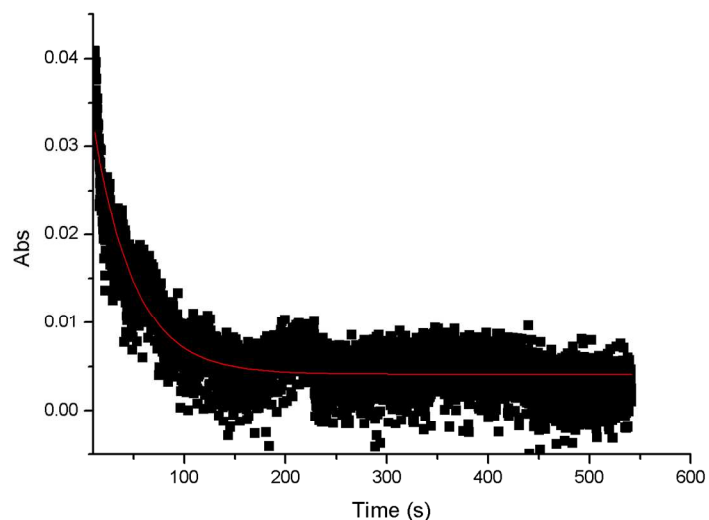


Figure S7. Representative pre-steady state kinetics trace the anaerobic reaction between Ferric SLO and protio-linoleic acid at 30 °C. The change in absorbance at 330 nm vs. time was measured on a desk top Cary50 spectrophotometer.

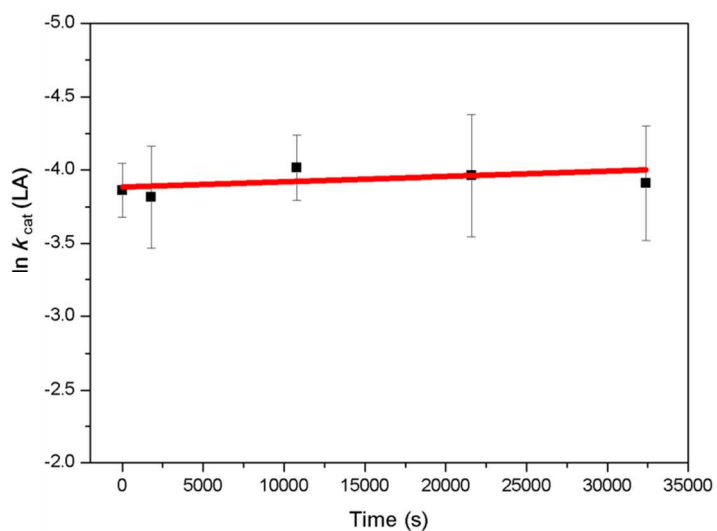


Figure S8. Assay for the stability of Ferric SLO under the condition of strict anaerobiosis in the glove box. This was conducted in the presence of a 2-fold excess of the product hydroperoxide (13-(*S*)-HPOD). At the indicated time points, enzyme was taken out of the glove box, diluted and assayed for activity with the protio-LA substrate.

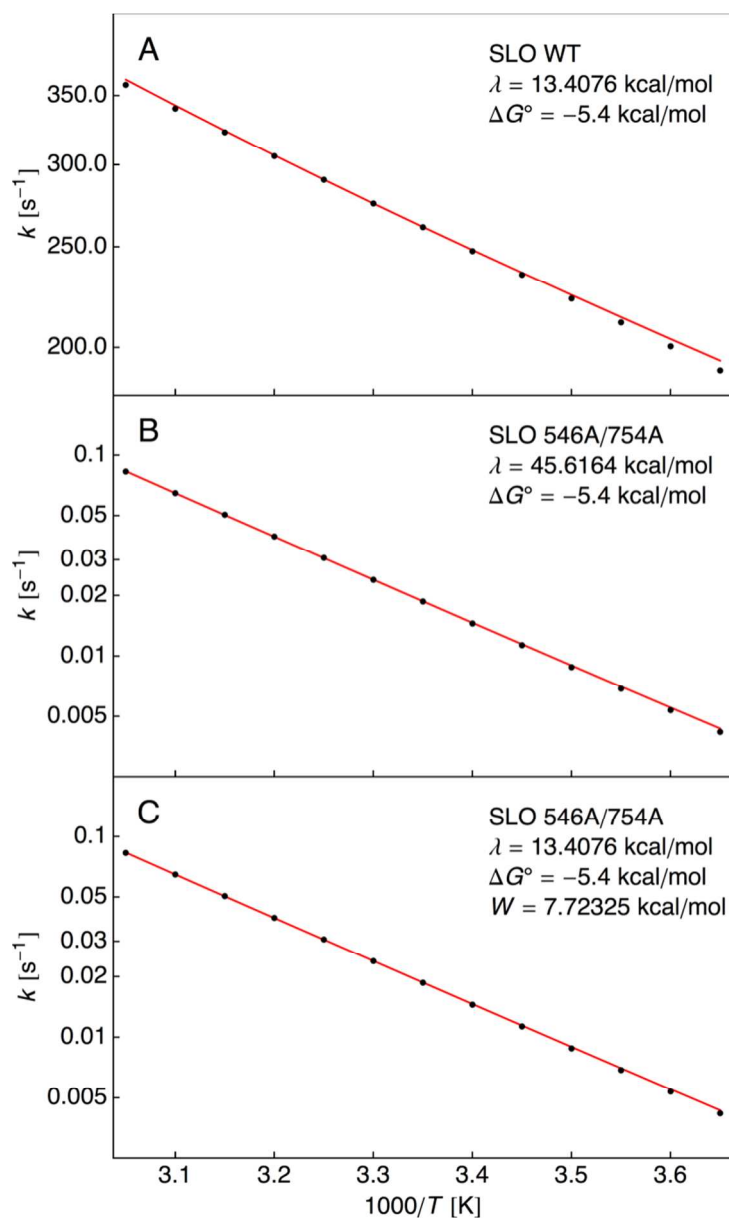


Figure S9. All of the “experimental data” (points, not actual experimental data) are obtained from the prefactor and apparent activation energy fit to the raw kinetic data for protio-LA. **(A)** Temperature dependence of the absolute rate constant for SLO WT. The theoretical curve is calculated using the high-temperature rate constant expression. **(B)** Temperature dependence of the absolute rate constant for DM SLO. The theoretical curve is calculated using the high-temperature rate constant expression with adjusted reorganization energy. **(C)** Temperature dependence of the absolute rate constant for the DM SLO. The theoretical curve is calculated using the high-temperature rate constant expression with a work term. For all of these plots, $\Omega = 174.574$ cm^{-1} and $R_{eq} = 2.709$ Å.

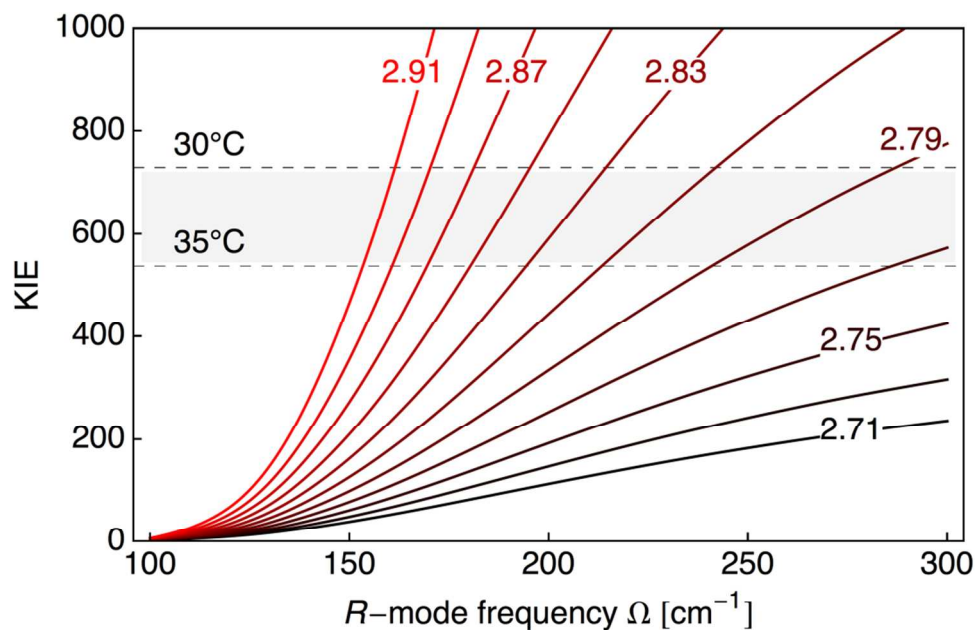


Figure S10. Predicted KIE for DM SLO as a function of the donor-acceptor equilibrium distance (R_{eq}) and the frequency of the donor-acceptor distance sampling (Ω). The curves are labeled according to R_{eq} given in Å. In this model, the reorganization energy is $\lambda = 13.408$ kcal/mol, the reaction free energy is $\Delta G^0 = -5.4$ kcal/mol and the additional work term is $W = 7.723$ kcal/mol. The region between the horizontally dashed lines corresponds to the experimental range of the observed KIEs at 35°C and 30°C.

III. Table S1-S4

Table S1. Empirical steady-state rate constants for DM SLO with protio-LA in 0.1 M borate, pH 9.0 as a function of temperature.^a

Temperature, °C	k_{cat} , s ⁻¹	k_{cat} error	K_{M} , μM	K_{M} error
10	0.007305	0.000430	17.8	2.3
15	0.010019	0.000675	12.7	1.9
20	0.012696	0.001350	11.3	2.5
25	0.016264	0.000951	12.5	1.8
30	0.020735	0.001079	8.07	1.4
35	0.030840	0.004056	14.5	3.8
40	0.040088	0.003531	13.9	4.8
45	0.048355	0.003295	13.8	2.7
50	0.064990	0.009117	23.8	6.4

^a Rates were determined in a continuous spectrophotometric assay.

Table S2. Proton donor-acceptor equilibrium distances and frequencies re-determined for WT and I553X mutants SLO using a λ value of 13.408 kcal/mol. These values, which were fit to both the magnitudes and temperature dependencies of the KIEs, are identical to those obtained in Ref. 15 with a significantly larger λ value.

Enzyme	R_{eq} [Å]	Ω [cm ⁻¹]
WT	2.709	174.574
I553V	2.76	156
I553L	2.85	133
I553A	2.82	140
I553G	2.94	128

Table S3. Non-adiabatic fittings for temperature dependence of the absolute rate constant for DM SLO with protio-LA as a function of assigned λ with R_{eq} and Ω fixed.

Enzyme	ΔG [kcal/mol]	λ [kcal/mol]	W [kcal/mol]	R_{eq} [Å]	Ω [cm ⁻¹]
WT	-5.4	13.408	0	2.709	174.574)
DM (Fit 1)	-5.4	45.616	0	2.709	174.574
DM (Fit 2)	-5.4	13.408	7.723	2.709	174.574

Table S4. X-ray data collection and refinement

	DM SLO
Data collection	
Space group	P 1 2 ₁ 1
Cell dimensions	
<i>a</i> , <i>b</i> , <i>c</i> (Å)	94.126 92.644 49.572
α , β , γ (°)	90 90.34 90
Resolution (Å)	66.03–1.7 (1.761–1.7)
<i>R</i> _{sym}	0.111 (0.70)
<i>I</i> / σ <i>I</i>	10.9 (1.6)
Completeness (%)	99.8 (100.0)
Redundancy	5.5 (3.7)
Refinement	
Resolution (Å)	1.7
No. reflections	666477 (28667)
<i>R</i> _{work} / <i>R</i> _{free}	0.1419 / 0.1752
No. atoms	
Protein	8275
Ligand/ion	61
Water	1021
B-factors	34.10
Protein	33.20
Ligand/ion	41.40
Water	40.00
R.m.s deviations	
Bond lengths (Å)	0.005
Bond angles (°)	1.01

IV. References

1. Sharma, S. C.; Klinman, J. P. *J. Am. Chem. Soc.* **2008**, *130*, 17632.
2. Rickert, K. W.; Klinman, J. P. *Biochemistry* **1999**, *38*, 12218.
3. Holman, T. R.; Zhou, J.; Solomon E. I. *J. Am. Chem. Soc.* **1998**, *120*, 12564.
4. Glickma, M. H.; Wiseman, J. S.; Klinman, J. P. *J. Am. Chem. Soc.* **1994**, *116*, 793.
5. Meyer, M. P.; Tomchick, D. R.; Klinman, J. P. *Proc. Natl. Acad. Sci. U.S.A.* **2008**, *105*, 1146.
6. Holton, J.; Alber, T. *Proc. Natl. Acad. Sci. U.S.A.* **2004**, *101*, 1537.
7. Leslie, A. G.; Powell, H. R. *Evolving Methods for Macromolecular Crystallography*, **2007**, *245*, 41.
8. Kabsch, W. *J. Appl. Crystallogr.* **1998**, *21*, 916.
9. Evans, P. *Acta Crystallogr. D Biol. Crystallogr.* **2006**, *62*, 72.
10. McCoy A. J. et al., *J. Appl. Crystallogr.* **2007**, *40*, 658–674.
11. Emsley, P.; Lohkamp, B.; Scott, W. G.; Cowtan, K. *Acta Crystallogr. D Biol. Crystallogr.* **2010**, *66*, 486.
12. Adams P. D. et al., *Acta Crystallogr. D Biol. Crystallogr.* **2010**, *66*, 213.
13. Hatcher, E.; Soudackov, A. V.; Hammes-Schiffer, S. *J. Am. Chem. Soc.* **2004**, *126*, 5763.
14. Lehnert, N.; Solomon, E. I. *J. Biol. Inorg. Chem.* **2003**, *8*, 294.
15. Skone, J. H.; Soudackov, A. V.; Hammes-Schiffer, S. *J. Am. Chem. Soc.* **2006**, *128*, 16655.
16. Hammes-Schiffer, S.; Soudackov, A. V. *J. Phys. Chem. B* **2008**, *112*, 14108.
17. Sirjoosingh, A.; Hammes-Schiffer, S. *J. Phys. Chem. A* **2011**, *115*, 2367.
18. Edwards, S. J.; Soudackov, A. V.; Hammes-Schiffer, S. *J. Phys. Chem. A* **2009**, *113*, 2117.
19. Hatcher, E.; Soudackov, A. V.; Hammes-Schiffer, S. *J. Am. Chem. Soc.* **2007**, *129*, 187.
20. Edwards, S. J.; Soudackov, A. V.; Hammes-Schiffer, S. *J. Phys. Chem. B* **2010**, *114*,

6653.

21. Marcus, R. A. *J. Phys. Chem.* **1968**, *72*, 891.

22. Marcus, R. A. *J. Am. Chem. Soc.* **1969**, *91*, 7224.